AUT Journal of Electrical Engineering

AUT J. Elec. Eng., 51(2) (2019) 153-160
DOI: 10.22060/eej.2019.16322.5285

Sensor-less Vector Control of a Novel Axial Field Flux-Switching Permanent-Magnet Motor with High-Performance Current Controller

J. Rahmani Fard*

Associate Professor, Electrical Engineering Department, Pooyesh Institute of Higher Education, Qom, Iran

ABSTRACT: Axial field flux switching motor with sandwiched permanent magnet (AFFSSPM) is a novel of flux switching motor. Based on the vector control method, the mathematical model of the AFFSSPM is derived and the operating performance of the AFFSSPM in the overall operating region is investigated. A novel control method for the AFFSSPM drive system, including the id =0, maximum torque per ampere, constant flux linkage, unity power factor control and flux-weakening strategy, is proposed. A prototype of the 12/19 poles AFFSSPM motor is manufactured and tested. Validity and feasibility of the proposed method were verified by experiments.

Review History:
Received: 2019-05-11
Revised: 2019-08-08
Accepted: 2019-08-18
Available Online: 2019-12-01

Keywords:
Flux-switching
Axial field
vector control
system drive

1. INTRODUCTION

Recently, suitable configuration and control strategy of the electric machines have been of the important research areas. Characteristics such as high-reliability, high-efficiency and better fault-tolerance capability are required for the EVs. Flux-switching permanent magnet (FSPM) motors attract an increasingly attention because of its features over conventional rotor-PM motors [1-6]. Although AFFSPM motors offer higher torque density, the torque density is restricted owing to decreased available winding space, because, in addition to the armature windings, the PMs are placed in the stator. Hence flux switching machines with sandwiched permanent magnet were suggested [7]. In each stator pole of flux switching sandwiched permanent magnet (FSSPM) motor two permanent magnets (PMs) are located, thus slot area is increased. Despite higher torque density, FSSPM machines present some disadvantages owing to their configurations such as asymmetric back-EMF, higher cogging torque and low fault-tolerant capability [8]. The axial flux-switching sandwiched permanent magnet (AFFSSPM) motor is a novel flux-switching motor which presents higher torque density, lower cogging torque and better fault-tolerant capability [9-10].

For the new structure of the Flux switching PM (FSPM) motor, AFFSSPM motor, the structural characteristics determine the particularity of its electromagnetic characteristics, and the corresponding control strategy which must be formulated for the characteristics of the motor. Among them, the current regulator is a key part of the motor control system, and the design of the current regulator directly affects the control effect of the motor torque and speed. The main purpose of this paper is to propose an improved current regulator control algorithm for the FSPM motor, so as to develop the most suitable control strategy for the motor. The proposed control method first apply the four current control methods of the constant torque region to the three-phase AFFSSPM motor. In the constant power region, the speed range is studied according to the field weakening control algorithm. When the motor speed is close to the set speed, in other words, the speed difference e(n) reaches the set speed threshold, the motor enters the constant torque zone. In this the speed regulator operates in the normal PI regulation state, and the torque command value is given according to the speed difference.

According to different current control algorithms, the rated torque and the rated speed of the motor are different. The rated speed and rated torque which can achieve are mutually constrained. Only suitable control algorithms can be selected according to different performance requirements.

When the motor speed reaches the turning speed and continues to rise, it enters the field weakening region. At this time, the motor terminal voltage has reached the inverter. The maximum voltage that can withstand. If the field weakening

*Corresponding author's email: javad.rahmani.fard@gmail.com

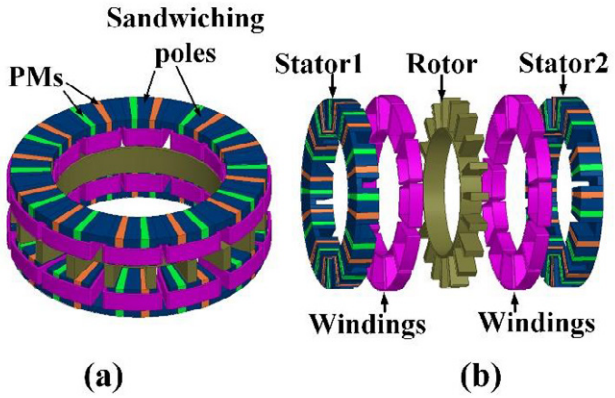

Fig. 1. Machine topology. (a) Configuration of the 12S/19 AFFSSPM. (b) 3D overview of the 12/19 AFFSSPM motor.

algorithm is not adopted, but the motor continues to work according to the current control algorithm of the constant torque region, the electromagnetic torque will drop rapidly.

However, to ensure the smooth transition of the motor from the constant torque region to the field weakening region, it is necessary to accurately determine the transition point. This paper is realized by real-time monitoring of the uq and ud voltages.

A novel control strategy for the AFFSSPM drive system, including the id =0, maximum torque per ampere, constant flux linkage, unity power factor control and flux-weakening strategy, is proposed. The sensor less control based on sliding mode observer is applied and the dynamic performance of AFFSSPM motor is investigated. The sliding mode observer (SMO) is used to estimate the rotor position and speed. Eventually, the validity and feasibility of the proposed method were verified by experiments.

2. AFFSSPM TOPOLOGY

Fig. 1(a) illustrates the configuration of 12/19 poles AFFSSPM motor, which consists of two outer stators and an inner rotor. Two PMs are imbedded in every stator pole with circumferentially magnetized direction alternately reversed in polarity. The lamination segment sandwiched between two PMs in a stator tooth is named as sandwiching pole. Fig. 1(b) illustrates the 3D overview of the 12/19 poles AFFSSPM motor.

2.1 Design Criteria

According to design concept as shown in Fig. 2, a particular combination of rotor poles and stator slots was derived as expressed in [10]. The number of rotor poles is

$$P_r = n_2\left(9n_1+1\right)/2 \tag{1}$$

and the number of slots in one stator for 3 phases is

$$S = 3n_1n_2 \tag{2}$$

where n_1 is defined as the number of coils for each phase group, n_2 is the number of groups for each phase. When the combination of $n_1=2$ and $n_2=2$ is selected, a 12/19 poles *AFFSSPM* motor is designed.

2.2 The AFFSSPM motor mathematical model

The voltage equations of *AFFSSPM* motor in d-q synchronous rotating reference frame may be expressed as

$$\begin{cases} u_d = R_{ph}i_d + \dfrac{\mathrm{d}\psi_d}{\mathrm{d}t} - \psi_q\omega_e \\ u_q = R_{ph}i_q + \dfrac{\mathrm{d}\psi_q}{\mathrm{d}t} + \psi_d\omega_e \end{cases} \tag{3}$$

where ψ_d is the d-axis flux, $\psi_d = L_di_d + \psi_m$, ψ_q is the q-axis flux, $\psi_q = L_qi_q$, u_d, u_q, i_d, i_q are d/q axes voltage and current, ω_e is the electrical angular velocity, ψ_m, R, L_d, L_q are permanent magnet flux linkage, stator resistance and d/q axes inductances. When the motor operates in steady state, u_d and u_q can be expressed as

$$\begin{cases} u_d = -\omega_eL_qi_q + R_{ph}i_d \\ u_q = \omega_eL_di_d + \psi_m\omega_e + R_{ph}i_q \end{cases}. \tag{4}$$

The electromagnetic torque in *AFFSSPM* motor can be expressed as:

$$T_{em} = \frac{3}{2}P_r\left(\psi_mI_msin\delta - \frac{1}{2}\left(L_d - L_q\right)I_m^2sin2\delta\right) \tag{5}$$

where δ is angle torque and for 12/19 *AFFSSPM* motor $L_d = L_q = L$.

3 PROPOSED CONTROL STRATEGY

For operating in the constant torque region below the base speed, the four current control methods (CM) including the $i_d=0$ (CM=1), maximum torque per ampere (CM=2), constant flux linkage (CM=3), unity power factor control (CM=4) and flux-weakening strategy are employed. When the rotational speed reaches the base speed, the flux-weakening control is adopted.

3.1 $\mathbf{i_d=0}$ control

In this method, the torque angle δ remains at 90°. Therefore, direct axis current can be obtained as

$$i_d = f_1\left(i_q\right) = 0 \tag{6}$$

Besides, the maximum quadrature axis current component with id=0 control is also:

$$\begin{cases} i_{dmax} = 0 \\ i_{qmax} = I_{max} \end{cases} \tag{7}$$

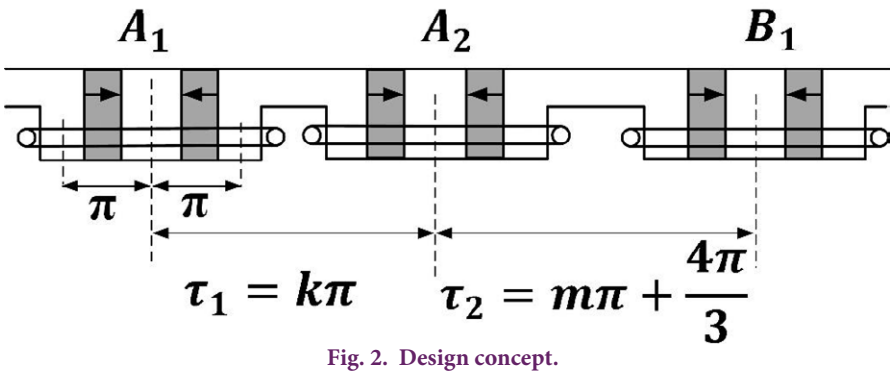

Fig. 2. Design concept.

3.2 Maximum torque per ampere control

This control method maximizes electromagnetic torque per current. It can be seen that in *AFFSSPM* motor $L_d < L_q$. Thus, the direct current can be obtained as follows [11,12]:

$$i_d = f_2\left(i_q\right) = \frac{\psi_m}{2\left(L_q - L_d\right)} - \sqrt{\frac{\psi_m^2}{4\left(L_q - L_d\right)^2} + i_q^2} \tag{8}$$

In addition, the maximum d and q current components are also as

$$\begin{cases} i_{dmax} = -I_{max} sin\delta = \dfrac{\psi_m}{4\left(L_q - L_d\right)} - \sqrt{\dfrac{\psi_m^2}{16\left(L_q - L_d\right)^2} + \dfrac{I_{max}^2}{2}} \\ i_{qmax} = \sqrt{I_{max}^2 - i_{dmax}^2} \end{cases} \tag{9}$$

3.3 Constant flux linkage control

In this control method, the resultant flux linkages of the stator d/q axes and rotor remains at a constant value. The direct axis current can be obtained as [13]

$$i_d = f_3\left(i_q\right) = \frac{-\psi_m + \sqrt{\psi_m^2 - L_q^2 i_q^2}}{L_d} \tag{10}$$

The d/q axes currents of the motor under the constant flux linkage control mode when the current reaches the limit value can be obtained:

$$\begin{cases} i_{dmax} = \dfrac{-L_d\psi_m + \sqrt{\psi_m^2 L_d^2 - \left(L_d^2 - L_q^2\right)L_q^2 I_{max}^2}}{\left(L_d^2 - L_q^2\right)} \\ i_{qmax} = \sqrt{I_{max}^2 - i_{dmax}^2} \end{cases} \tag{11}$$

3.4 Unity power factor control ($\cos\varphi = 1$)

A $cos\varphi = 1$ control implies that the apparent power rating of the inverter is entirely employed for the real power input to the *AFFSSPM* motor. The direct axis current can be obtained as [14]

$$i_d = f_4\left(i_q\right) = \frac{-\psi_m + \sqrt{\psi_m^2 - 4L_d L_q i_q^2}}{2L_d} \tag{12}$$

The d/q axes currents when the motor reaches the limit value under $cos\varphi = 1$ control can be obtained as

$$\begin{cases} i_{dmax} = \dfrac{\psi_m - \sqrt{\psi_m^2 - 4\left(L_d - L_q\right)L_q I_{max}^2}}{2\left(L_q - L_d\right)} \\ i_{qmax} = \sqrt{I_{max}^2 - i_{dmax}^2} \end{cases} \tag{13}$$

3.5 Flux-weakening control

when the motor is running above the base speed, the inverter voltage reaches the limit value. Thus, the motor is operating under flux-weakening control. The direct current can be obtained as follows [16]

$$i_d = f_5\left(i_q, \omega_e\right) = \frac{-\psi_m + \sqrt{\dfrac{U_{max}^2}{\omega_e^2} - L_q^2 i_q^2}}{L_d} \tag{14}$$

where U_{max} is maximum phase voltage value and is equal to $U_{dc}/\sqrt{3}$ and U_{dc} is the dc link voltage. Besides, the maximum d and q current components are also as

$$\begin{cases} i_{dmax2} = \dfrac{L_d\psi_m - L_q\sqrt{\psi_m^2 + \left(L_q^2 - L_d^2\right)\left(I_{max}^2 - \dfrac{U_{max}^2}{\omega_e^2 L_q^2}\right)}}{\left(L_q^2 - L_d^2\right)} \\ i_{qmax2} = \sqrt{I_{max}^2 - i_{dmax2}^2} \end{cases} . \tag{15}$$

3.6 Proposed control method for 12/19 AFFSSPM motor

1. From the reference torque T_{em}^*, regardless of the reluctance torque, the i_q is calculated.
2. According to different current control method (CM =

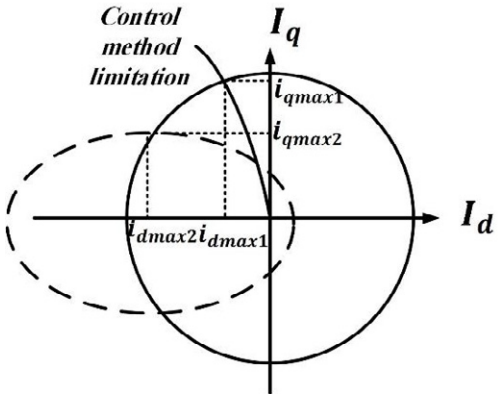

Fig. 3. Principle of proposed method.

1, 2, 3, 4), the electromagnetic motor parameters (permanent magnet flux linkage ψ_m, dq -axes inductances L_d, L_q, winding resistance per phase R_{ph}) and inverter limitations (U_{max} and I_{max}) are substituted into the Eqs. ((7), (9), (11), (13)) to obtain idmax1, iqmax1 at the base speed.

3. Compare i_q and iqmax1. If $i_q > i_{qmax1}$, it means that the given value is outside of the current circle, and i_{dmax1}, i_{qmax1} can be directly assigned to i_d and i_q. If $i_q < i_{qmax1}$, the i_q is used as an independent variable to obtain id based on the different equations of the four current control methods (Eqs. (6), (8), (10), (12)).

4. According to the voltage Eq. (4), u_d and u_q are calculated based on above i_q and i_d.

5. The voltage of the motor terminal u0 is obtained from the u_d and u_q. It is compared with the voltage limitation U_{max}. If the motor is operating in the constant torque region, the current controller is not saturated. So directly the above currents are considered as reference values for i_d^*, i_q^*.

6. If $u_0 > U_{max}$, the current controller is saturated and enters the field-weakening region. The i_{dmax2}, i_{qmax2} are calculated according to Eq. (15).

7. Compare i_q and i_{qmax2}. If $i_{qmax2} < i_q$, assign i_{dmax2} and i_{qmax2} to i_d and i_q, respectively. If $i_{qmax2} > i_q$, as shown in Fig.3, according to the Eq. (14), the i_d is calculated. Then the above currents are considered as the i_d^*, i_q^*. This current control strategy flowchart is shown in Fig.4.

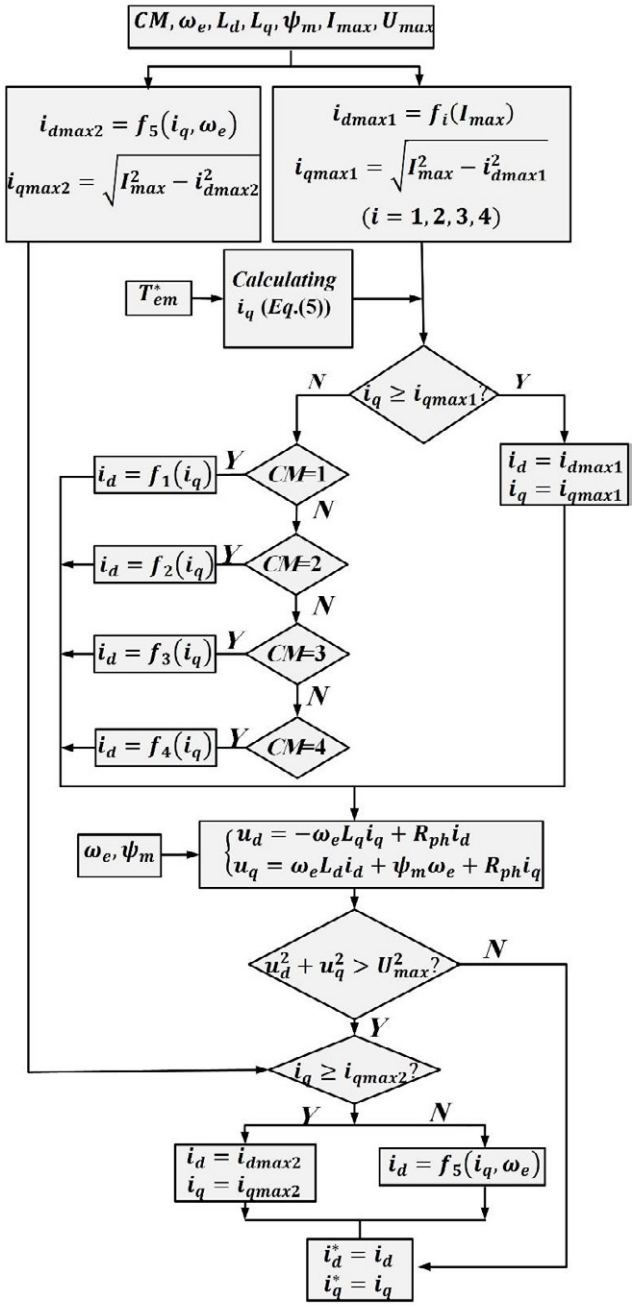

Fig. 4. Flowchart of the proposed current control method.

3.7 Position and Speed Estimation Based on Sliding Mode Observer

A position and speed estimation based on sliding mode observer are presented in [16]. This principle is shown in Fig 5. The phase-locked loop technology (PLL) is used to estimate the speed.

The block diagram of the 12/19 *AFFSSPM* motor control with the proposed controller is shown in Fig.6.

4. CO-SIMULATIONS RESULTS

We appreciate the reviewer's comment. In this study, we use Co-Simulation to investigate the performance of the proposed method. Certainly, a simple linear model is not sufficient for a precise analysis. If the magnetic saturation and time/space harmonics and etc. have been considered, the motor model will be nonlinear and analysis will be much closer to reality.

In this study, firstly, we provide the 3-D FEM model of the proposed motor in the"MAXWELL 16" software. Then, In order to create the electrical and electromechanical parts of drive system the "ANSYS SIMPLORER" software is employed. Finally, the control algorithm of the drive system is implemented in "Simulink/MATLAB".

The Co-Simulation lets us analysis of the motor with 3-D finite element method, external drive circuit and control system at the same time.

The Fig. 8 shows the simulation waveform of the AFFSSPM motor based on proposed. The given speed is 100 rpm, and

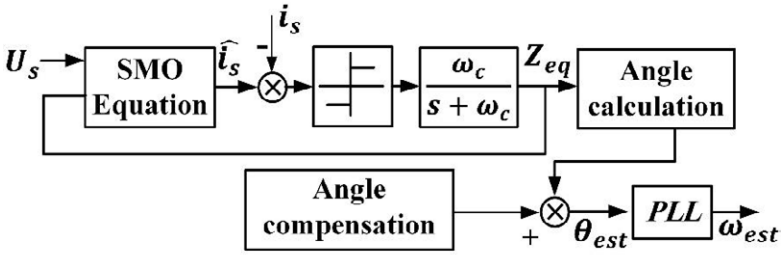

Fig. 5. Position and speed estimation based on sliding mode observer.

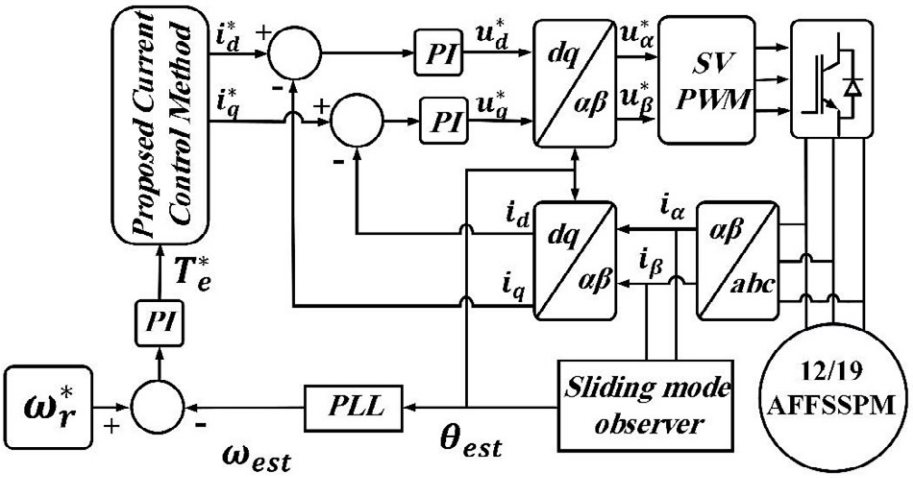

Fig. 6. The scheme for 12/19 AFFSSPM motor control with proposed controller.

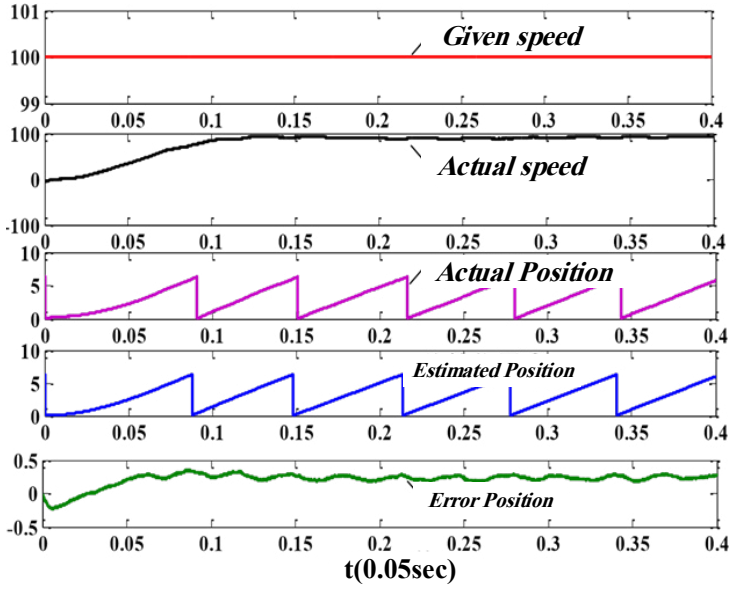

Fig.7. Proposed method without position control simulation waveform

the motor starts from zero speed. In the process of quick start, it can be seen that the position tracking performance is good, and the position error at the steady state is at most 15 degrees.

5. EXPERIMENTAL RESULTS

In order to verify the validity of the proposed control strategy and investigate the operating performance of the 12/19 poles *AFFSSPM* motor the experiments are done by a DS1104 DSP. The parameters of the experimental system are listed in Table 1. Fig. 8 illustrates the 12/19 poles *AFFSSPM* motor and the experimental setup.

Fig. 9(a) shows the position control waveforms of the motor with sliding mode observer method. It can be seen that the estimated position can be well compared with the

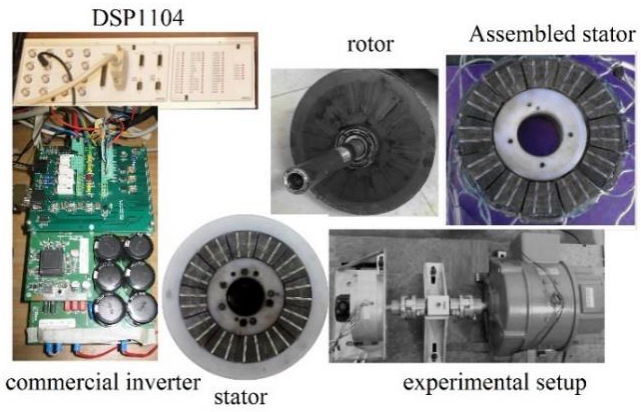

Fig.8. Experimental setup

Table 1: Main parameters of the investigated machine.

Parameter	value
Stator resistance R_{ph} / Ω	0.65
d axis inductance L_d / mH	10
q axis inductance L_q / mH	10
Rotor flux ψ_m / Wb	0.1
Rated speed n / rpm	200
Rated torque T_n / $N.m$	12
Rated power P / kW	0.75
dq axes rated current Id=Iq/ A	10
Sampling time T/ s	10^{-4}
DC link voltage U_{dc}/V	200

actual position and the position error is small, about 10°. Fig. 9(b) shows the position control waveforms when the 12/19 *AFFSSPM* motor rotates in forward and reverse directions. The estimated position can still track the actual position with low error.

Fig. 10 shows the initial position tracking. The initial rotor position is 54°. It can be seen that the tracking time is 30ms.

The experimental results of dynamic characteristics for the 12/19 *AFFSSPM* motor are shown in Fig.11. First, the load torque is 12N.m and accelerated from 0 speed to 200 r/min. Suddenly, the load is removed at 0.4s and the motor is no load. The reference speed changes to 240 r/min at 0.5s. The load torque changes to 1.5N.m at 0.8s. The id=0 control is activated at the starting and the control method is changed to maximum torque per ampere control at 0.2s.

It can be seen that the actual speed as well as the reference speed. After removing the load torque, the electromagnetic torque is merely to overcome the cogging torque and the mechanical friction losses. As can be seen, after changing the control method from id=0 to maximum torque per ampere method, the torque and speed are still smooth and ripple is small.

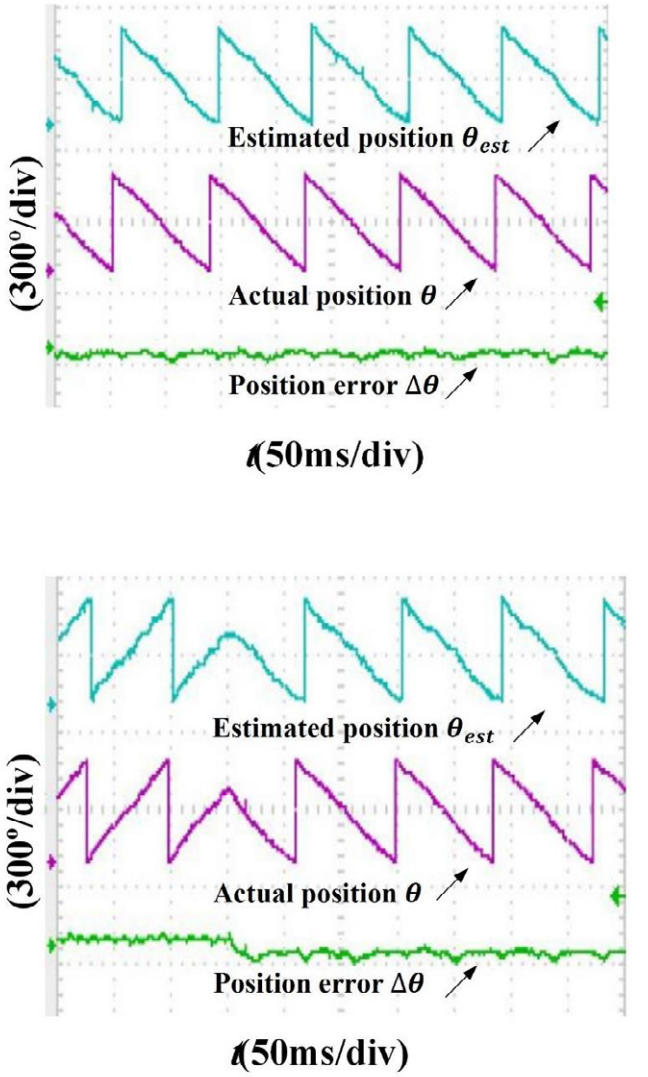

Fig. 9. (a)Position control waveforms of the motor. (b) Position control waveforms when the motor rotates in forward and reverse directions.

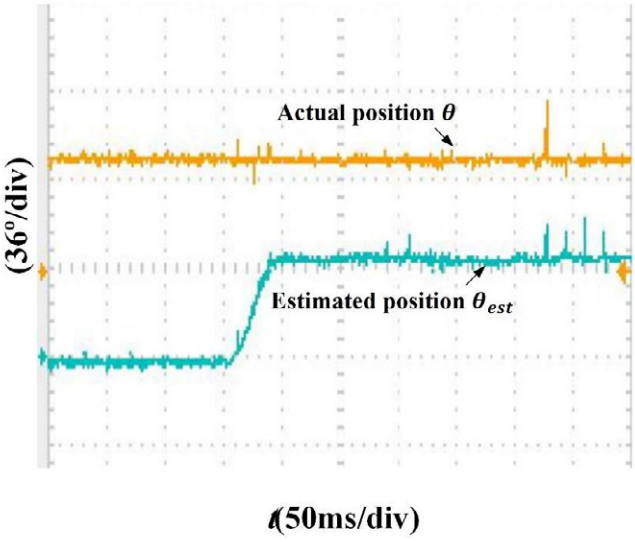

Fig. 10. Initial position tracking.

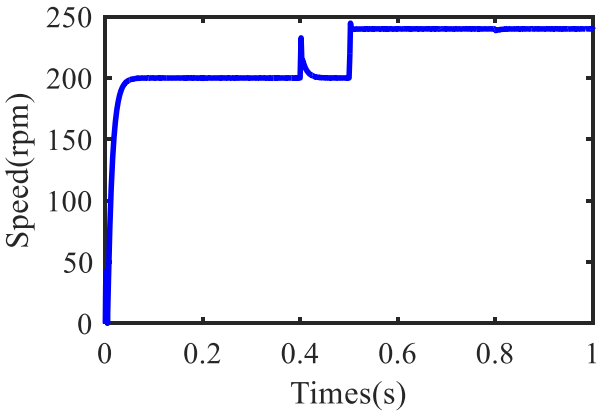

(a)

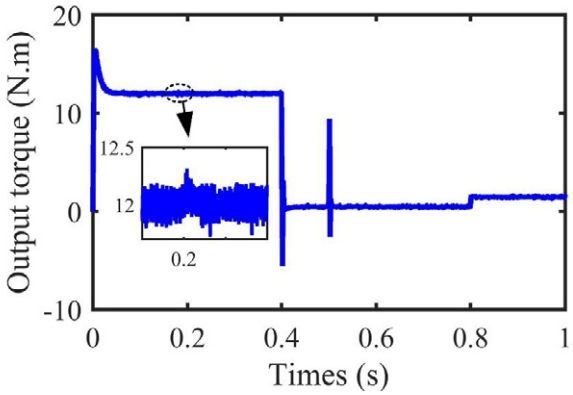

(b)

Fig. 11. (a) Motor speed (b) Output torque

6. CONCLUSION

In this paper, a vector control scheme has been developed to investigate the performance of the 12/19 *AFFSSPM* motor in the entire operating region. Moreover, a sensor less control based on sliding mode observer is applied. To evaluate the performance of the *AFFSSPM* motor, a prototype of the 12/19 poles *AFFSSPM* motor is manufactured and tested. Experimental results show dynamic performance is excellent also torque and speed ripples are low and the system has high reliability.

REFERENCES

[1] M. Cheng, W. Hua, J. Zhang, W. Zhao, Overview of stator-permanent magnet brushless machines, IEEE Transactions on Industrial Electronics, 58(11) (2011) 5087-5101.

[2] A. Thomas, Z. Zhu, G. Jewell, Comparison of flux switching and surface mounted permanent magnet generators for high-speed applications, IET Electrical Systems in Transportation, 1(3) (2011) 111-116.

[3] Z. Zhu, Y. Pang, D. Howe, S. Iwasaki, R. Deodhar, A. Pride, Analysis of electromagnetic performance of flux-switching permanent-magnet machines by nonlinear adaptive lumped parameter magnetic circuit model, IEEE Transactions on magnetics, 41(11) (2005) 4277-4287.

[4] Y. Wang, M. Jin, W. Fei, J. Shen, Cogging torque reduction in permanent magnet flux-switching machines by rotor teeth axial pairing, IET electric power applications, 4(7) (2010) 500-506.

[5] J. Chen, Z. Zhu, S. Iwasaki, R.P. Deodhar, A novel E-core switched-flux PM brushless AC machine, IEEE Transactions on Industry Applications, 47(3) (2011) 1273-1282.

[6] Z. Zhu, J. Chen, Y. Pang, D. Howe, S. Iwasaki, R. Deodhar, Analysis of a novel multi-tooth flux-switching PM brushless AC machine for high torque direct-drive applications, IEEE Transactions on Magnetics, 44(11) (2008) 4313-4316.

[7] W. Fei, J. Shen, Novel permanent magnet switching flux motors, in: Proceedings of the 41st International Universities Power Engineering Conference, IEEE, 2006, pp. 729-733.

[8] K. Lu, P.O. Rasmussen, S.J. Watkins, F. Blaabjerg, A new low-cost hybrid switched reluctance motor for adjustable-speed pump applications, IEEE Transactions on Industry Applications, 47(1) (2010) 314-321.

[9] Y. Zhou, Z. Zhu, Torque density and magnet usage efficiency enhancement of sandwiched switched flux permanent magnet machines using V-shaped magnets, IEEE Transactions on Magnetics, 49(7) (2013) 3834-3837.

[10] J.R. Fard, M. Ardebili, Design and prototyping of the novel axial flux-switching permanent-magnet motor, COMPEL-The international journal for computation and mathematics in electrical and electronic engineering, (2018).

[11] S. Morimoto, M. Sanada, Y. Takeda, Wide-speed operation of interior permanent magnet synchronous motors with high-performance current regulator, IEEE Transactions on Industry Applications, 30(4) (1994) 920-926.

[12] A. Consoli, G. Scarcella, G. Scelba, A. Testa, Steady-state and transient operation of IPMSMs under maximum-torque-per-ampere control, IEEE transactions on Industry Applications, 46(1) (2009) 121-129.

[13] R. Krishnan, Permanent magnet synchronous and brushless DC motor drives, CRC press, 2017.

[14] M. Moussa, A. Helal, Y. Gaber, H. Youssef, Unity power factor control of permanent magnet motor drive system, in: 2008 12th International Middle-East Power System Conference, IEEE, 2008, pp. 360-367.

[15] Y. Inoue, S. Morimoto, M. Sanada, Comparative study of PMSM drive systems based on current control and direct torque control in flux-weakening control region, IEEE Transactions on Industry Applications, 48(6) (2012) 2382-2389.

[16] J.R. Fard, M. Ardebili, Design and control of a novel yokeless axial flux-switching permanent-magnet motor, IEEE Transactions on Energy Conversion, 34(2) (2018) 631-642.

HOW TO CITE THIS ARTICLE

J. Rahmani Fard, Sensor-less Vector Control of a Novel Axial Field Flux-Switching Permanent-Magnet Motor with High-Performance Current Controller, AUT J. Elec. Eng., 51(2) (2019) 153-160.

DOI: 10.22060/eej.2019.16322.5285